

New concept of a 3D-probing system for micro-components

T. Liebrich*, W. Knapp (1)

inspire/Institute of Machine Tools and Manufacturing (IWF), ETH Zurich, Tannenstrasse 3, CLA G11.2, 8092 Zurich, Switzerland

ARTICLE INFO

Keywords:
Metrology
Sensor
Interferometry

ABSTRACT

The results of a feasibility study with the aim to demonstrate the applicability of a Fizeau interferometer for tactile dimensional metrology are presented. The concept is based on a Fizeau interferometer for detecting the deflection of an internal measuring plane at which the probing stylus is attached. The mechanical setup is dimensioned for small probing forces and an isotropic probing behaviour. Results and experience during building up the probing system and evaluating the interference images are presented. Furthermore, the advantages and disadvantages of the new 3D-probing concept with a theoretical resolution of 0.1 μm (X -/ Y -direction) and 0.04 μm (Z -direction) are discussed.

© 2010 CIRP.

1. Applicability of Fizeau Interferometry for 3D-probing concept

Progress in miniaturisation of components requires dimensional micro- and nanometrology [1]. The presented probing system is based on a Fizeau interferometer [2,3], which is normally used in surface testing [4]. The information given by the interference pattern is the orientation of the surface under test relative to the reference surface as well as the form deviation of the surface under test relative to the reference surface.

In this application, the orientation of the surface under test is directly associated with the deflection of the probing sphere (see Fig. 1). Deflecting the probing sphere causes a change in the orientation and the distance of the interference fringes.

By evaluating the orientation of the moveable surface under test relative to the non-moveable reference surface, the position of the probing sphere can be calculated, if the length of the probing stylus is calibrated. Additionally, an undesired deformation of the surface under test, caused by too high probing forces, can be detected in the interference pattern. A Z -translation of the probing sphere changes the interference pattern over the whole diameter of the laser beam only in its intensity, but not in its shape. This has to be detected by an online evaluation, which will be implemented in a future work. The surface under test is suspended by flexure hinges, so that a translation in Z -direction and the two rotations A and B are its degrees of freedom (see Fig. 1). With only one sensor, the X -, Y - and Z -position of the probing sphere can be determined.

2. Design and theoretical performance of the probing head

An advantage of the probing system is the simple mechanical setup, as shown in Fig. 1.

2.1. Setup of the probing head and test stand for probing head

The setup of the test stand is shown schematically in Fig. 2. The main components are the laser interferometer, the adjustment unit and the probing head. The probing behaviour is determined by the probing head, at which the probing stylus is mounted. The moveable part of the probing head is elastically supported by flexure hinges, which are manufactured by laser cutting from a thin foil with adequate thickness of 0.06 mm (red part in Fig. 3) and then connected by laser welding with the fixed part of the probing system (green part in Fig. 3). The manufactured probing head is shown in Fig. 4. The flexure hinges, the non-moveable suspension and the moveable adaptor for the probing stylus are assembled by crosswise laser spot welding to minimise the inserted energy into the assembly. The welding process ensures a positive locking between the different components.

2.2. Simulation of probing behaviour

In order to enable an application of the probing system for micro-components, the probing force has to be in the range of a few mN or even less [5–7]. Otherwise, probing spheres with diameters typically smaller than 500 μm damage the workpiece to be checked because then the Hertzian pressure is too high [5,8]. For this reason, the influence of the geometry and the material of the flexure hinges on the probing behaviour are simulated with FEM. The resulting geometry is shown in Figs. 3 and 4. The material of the three components is stainless steel 1.4310. The flexure hinges have a length of 11 mm, a width of 0.6 mm and a thickness of 0.06 mm. The design has a low stiffness in direction of the intended movements (Z , A , B) and a high stiffness in direction of the non-intended movements (X , Y , C) (see Fig. 3). The mechanical properties are summarised in Table 1. With this design, low contact forces during probing as well as a large measurement range of the probing system ($\sim 100 \mu\text{m}$) are realised.

* Corresponding author.

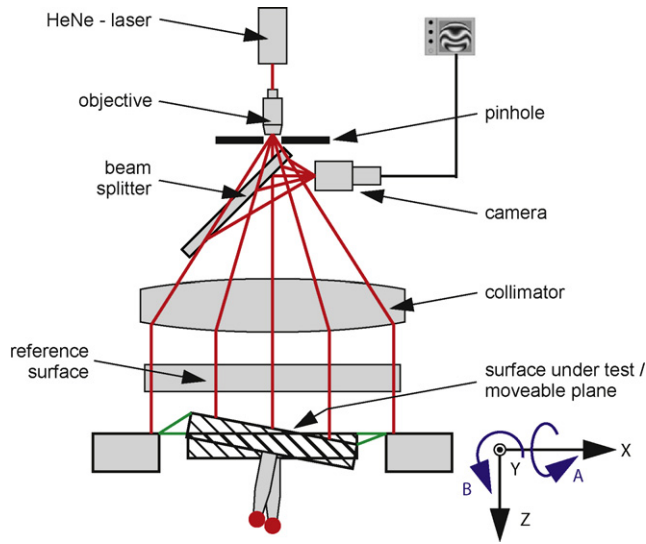


Fig. 1. Setup for 3D-probing system.

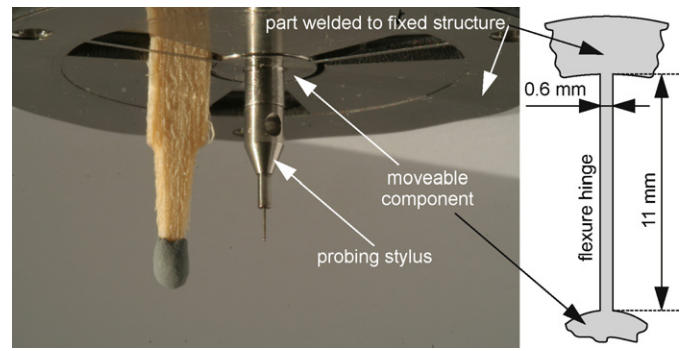


Fig. 4. Manufactured probing head with match for comparing the scale and dimensions of the flexure hinges.

Table 1

Mechanical properties of the flexure hinges (FEM simulations).

Stiffness in X and Y ^a at tip of the probe	18.9 N/mm
Stiffness in Z ^a at tip of the probe	0.06 N/mm
Stiffness around A and B ^a	0.058 Nmm/°
Critical deflection of the sphere (von Mises criteria)	0.48 mm
Probing force for deflection of the sphere of 10 μm	0.2 mN
Eigenfrequencies (1st/2nd)	35.7/82.9 Hz
Moving mass	1.1 g

^a Definition of coordinate system: see Fig. 3.

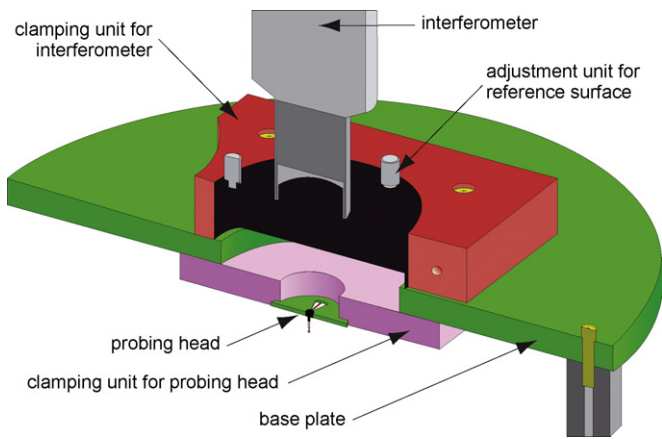


Fig. 2. Sectional view of test stand for the probing system.

3. Properties of the probing system

The simulated properties are checked by different experiments, which are discussed in this section.

3.1. Checking of probing behaviour

The probing behaviour in X- and Y-direction is checked with stiffness measurements: a force sensor is mounted on a manual positioning device, whose deflection is determined by a 1D-length measuring device. The force sensor is in contact with the probing sphere and measures the probing force for deflections of the

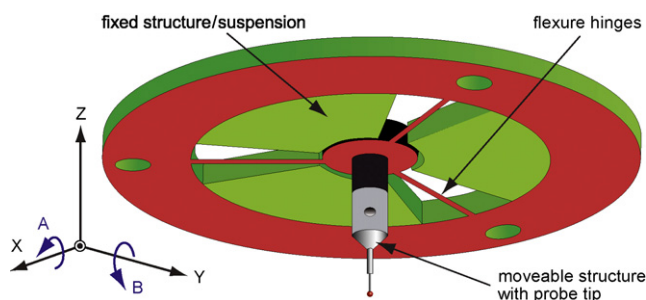


Fig. 3. Resulting geometry of the flexure hinges for the 3D-probing concept.

probing sphere from 0.06 mm up to 0.24 mm. The direction of deflecting the probing sphere is changed in steps of 30°. The results are shown in a polar plot (see Fig. 5). For a fixed deflection of the probing sphere, the measured probing force is almost independent of the direction of the deflection. Thus, the simulated anisotropy could be experimentally shown.

Contrary to simulations, the measured probing forces are much higher (up to a factor of 30, dependent on which probing head is checked). This is caused by the manufacturing of the flexure hinges (as explained in Section 3.2) and is repetitive for all three checked probing heads.

3.2. Influence of process parameters during manufacturing

In order to explain the differences in probing forces between simulation and experiment, the flexure hinges are investigated

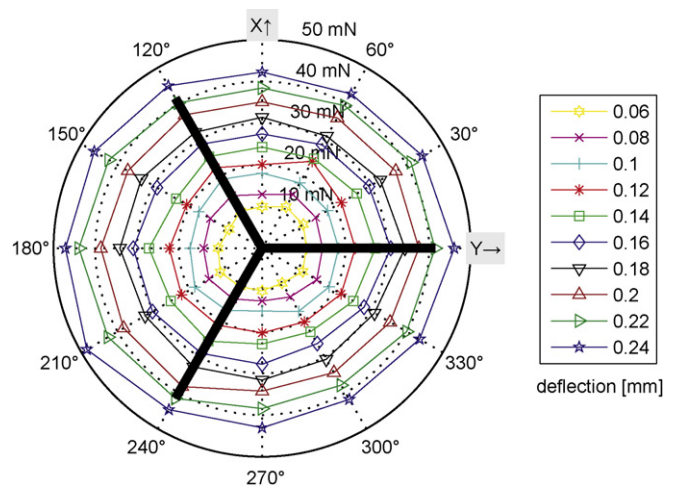


Fig. 5. Checking the anisotropy of the probing system in XY-plane by measuring the probing force (radial, 0–50 mN) for an adjusted deflection of the probing sphere (different line style) in dependence of the direction of deflection (azimuthally from 0° to 360°, bold line: location of flexure hinges) (uncertainty of force measurement $U(k=2) < 2$ mN).

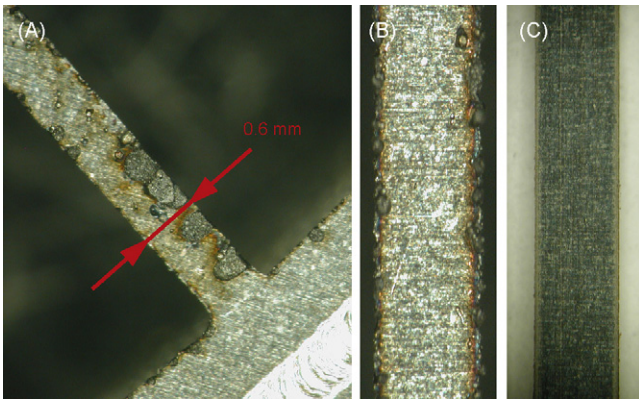


Fig. 6. Influence of manufacturing parameters on cutting edge of flexure hinges (A and B: burrs and burn marks. C: no burrs and burn marks with optimised cutting parameters at bending beam).

with an optical 3D-microscope based on focus variation. The flexure hinges are manufactured by laser cutting. Process parameters such as cutting speed, focal position, pressure of process gas or laser power has great influence on the quality of the cut and on the cutting area. Because these parameters have not been optimised for cutting the 0.06 mm thick stainless steel, burrs as well as burn marks along the cutting edge have been generated (see Fig. 6). The burr has an average height of approximately $20\ \mu\text{m}$ and a width of approximately $40\ \mu\text{m}$. This causes an increase of the stiffness, because the geometrical moment of inertia is increased. The resulting influence on the stiffness has been computed and is consistent with the measured differences. In order to minimise potential influences from varying material properties or manufacturing parameters, a simple bending beam is manufactured under optimised process parameters. The calculated and measured stiffness are $0.017\ \text{N/mm}$ and $0.016\ \text{N/mm}$, respectively. In this way, an easy and fast check is implemented to verify the assumptions of the calculations before the probing head is assembled [9].

3.3. Software for evaluating the position of the probing sphere

The relevant information about the position of the probing sphere is enclosed in the interference images. A deflection of the probing sphere causes a change in the phase of the light wave between reference beam and measurement beam. Thus an intensity modification of the superposed beam is generated, which results in a changing interference pattern [3,10]. Consequently, the

maximum speed of deflecting the probing sphere is limited by the speed of the image processing. The direction of deflecting the probing sphere is given by the orientation of the interference fringes; the magnitude of the deflection is inversely proportional to the distance between the interference fringes.

In a first step, an algorithm for determining the relative shift between two images is realised. The intention is to prove that the deflection of the probing sphere can be determined using a Fizeau interferometer. Actually, the image processing speed is very low, because the resolution of the interferometer is very high (480×640 pixels). This shall be improved in the next step. The implementation of an online measurement of the Z-movement shall be also realised in the next step. Therefore another optical system is needed, which enables image processing with at least 25 kHz for opportunity of scanning [5].

The main modules of the current algorithm are the following:

- Filtering the image in order to reduce noise.
- Edge detection in the intensity image.
- Detection of lines of the interference fringes by using Hough transform [11]. Their orientation is compared with an optimisation, which minimises the distance of intensity peaks on a section through the interferogram.
- The result is used for calculating the out-of-plane tilting of the surface under test referred to the reference surface.
- The distance between fringes in the interferogram is determined.
- Calculating the position of the probing sphere.

The output for detecting the axis of rotation by minimising the distance of the intensity peaks is shown in Fig. 7.

The developed algorithm is checked with simulated interference images between a perfect flat reference surface and a perfect flat surface under test: the sinus profile of the intensity is preset, so the orientation of the interference fringes and the distance between themselves are known. The interference images are simulated directly, without any connection to the evaluation algorithm to be checked.

3.4. Measurements results

The presented results are only for deflecting the probing sphere horizontally. In future investigations, real 3D-measurements of a test part are planned to determine the sensitivity and stability of the probing system in more detail. The relative deflection of the probing sphere between two images is determined with the algorithm as described above and compared with the deflection measured by an additional 1D-length measuring device. Before, the stylus length is calibrated by minimising the differences between the detected deflections by the two devices.

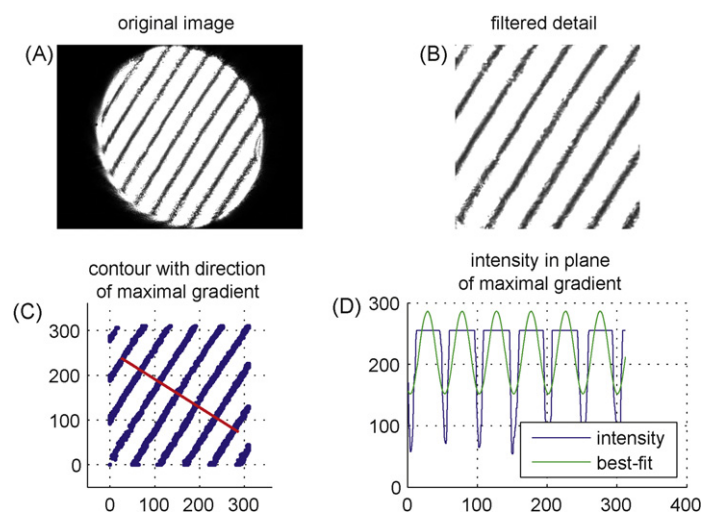


Fig. 7. Determining the orientation of the surface under test (results of single steps shown in image A–D).

Table 2
Results of displacements measurements (measurement uncertainty $U(k=2)$).

Detected deflection [μm] by		Relative error [%]
1D-length measuring device	3D-probing system	
2.6 ± 0.23	2.42 ± 0.24	7.4 ± 12.8
5.7 ± 0.23	5.60 ± 0.24	1.8 ± 5.8
9.0 ± 0.23	8.87 ± 0.24	1.5 ± 3.7
13.5 ± 0.23	13.48 ± 0.24	0.1 ± 2.5
19.9 ± 0.24	19.94 ± 0.24	0.2 ± 1.7
25.7 ± 0.24	25.78 ± 0.24	0.3 ± 1.3
Measurement 2 with separate calibration		
3.4 ± 0.23	3.44 ± 0.24	1.2 ± 9.8
10.3 ± 0.23	10.47 ± 0.24	1.7 ± 3.2
19.1 ± 0.24	19.12 ± 0.24	0.1 ± 1.8
22.3 ± 0.24	22.19 ± 0.24	0.5 ± 1.5

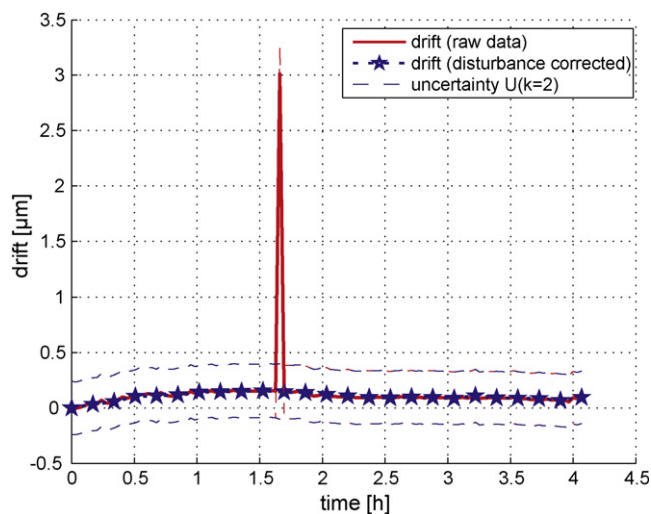


Fig. 8. Thermal drift of 3D-probing system if probing sphere is freestanding (measurement uncertainty $U(k=2)$: $\pm 0.24 \mu\text{m}$, see dashed lines).

The principal contributors to the measurement uncertainty of the 1D-length measuring device are the measuring uncertainty of the incremental probe ($\pm 0.2 \mu\text{m}$ over 12 mm measuring range) and the angular error of the probing direction from the deflecting direction (assumption: range $\pm 1.5^\circ$). The thermal drift is neglected, because the measurement period is smaller than 1 min and the whole setup is temperature conditioned for at least 4 h. The measurement uncertainty is $U(k=2) = 0.24 \mu\text{m}$ for length $\leq 0.24 \text{ mm}$.

The principal contributors to the measurement uncertainty of the 3D-probing system are the uncertainty of the interferometer and the performance of computing the orientation of the surface under test. For the fitting of the line with maximal gradient used in Fig. 7C, a 95% confidence interval is calculated. The uncertainty of the interferometer with the used reference surface is according to the manufacturer instruction $\lambda/10$, which results in a standard uncertainty at the probing sphere in horizontal direction of $0.11 \mu\text{m}$. The total measurement uncertainty is $U(k=2) = 0.24 \mu\text{m}$ for length $\leq 0.24 \text{ mm}$. The thermal drift is neglected for the same reason as described above. The results are summarised in Table 2. The direction of deflecting the probing sphere has no influence on the detected deflection.

The repeatability of the probing system is determined to be $0.19 \mu\text{m}$. This standard deviation is almost as large as the

estimated uncertainty of the 1D-length measuring device, which is used to deflect repetitively the probing sphere. Consequently, the checking of the 3D-probing system is currently limited by the used 1D-length measuring device and the manual positioning device.

The drift has also been measured. For a measurement period of 4 h the thermal drift is determined to be $0.16 \mu\text{m}$ (see Fig. 8). The peak in Fig. 8 (red curve) is caused by disturbances, e.g. persons walking through the laboratory, and is eliminated for the drift evaluation (blue curve in Fig. 8). If the probing system is calibrated each 30 min, the drift can be reduced to $0.1 \mu\text{m}$. During drift measurements, the probing sphere is not in contact with a workpiece. The test conditions are typical laboratory conditions with air conditioning to $20 \pm 0.5 \text{ }^\circ\text{C}$.

4. Conclusion

A new 3D-probing system for tactile coordinate metrology has been presented. The concept is based on a Fizeau interferometer, which detects the deflection of an internal measuring plane at which the probing sphere is fixed. The anisotropy during deflecting the probing sphere is experimentally proven. The difference between calculated and measured stiffness of the flexure hinges is caused by burr formation during manufacturing the flexure hinges. With optimised machining parameters a simple bending beam is manufactured and correspondence to simulation is proven. The properties of the material used as well as the manufacturing can be checked before the components of the probing head are assembled.

The applicability of a Fizeau interferometer for tactile probing systems is shown:

- Thermal drift smaller than $0.16 \mu\text{m}$ over 4 h in usual laboratory condition (air conditioned to $20 \pm 0.5 \text{ }^\circ\text{C}$).
- Anisotropy of the direction of deflecting the probing sphere in XY-plane.
- Independent check of evaluated deflection.

Based on the results and experience of the feasibility study, the probing system will be improved and expanded to a high dynamic system. The costs of the probing system are mainly caused by the laser interferometer and not by the manufacturing process of the used components, because conventional manufacturing processes like laser cutting, laser welding or drilling are used.

References

- [1] Hansen HN, Carneiro K, Haitjema H, De Chiffre L (2006) Dimensional Micro and Nano Metrology. *Annals of the CIRP* 55(2):721–743.
- [2] Hariharan P (2007) *Basics of Interferometry*. Academic Press. ISBN-10: 0-12-373589-0.
- [3] Hariharan P (2003) *Optical Interferometry*. Elsevier 978-0-12-311630-7.
- [4] Jansen MJ, Haitjema H, Schellekens PHJ (2006) Development of a Double Sided Stitching Interferometer for Wafer Characterization. *Annals of the CIRP* 55(1):555–558.
- [5] Weckenmann A, Estler T, Peggs G, McMurtry D (2004) Probing Systems in Dimensional Metrology. *Annals of the CIRP* 53(2):657–684.
- [6] Meli F, Küng A (2004) Performance of a Low Force 3D Touch Probe on an Ultraprecision CMM for Small Parts. *Proceedings of the 4th Euspen Conference*, 270–271.
- [7] Küng A, Meli F, Thalmann R (2007) Ultra Precision Micro-CMM Using a Low Force 3D Touch Probe. *Measurement Science and Technology* 18:319–327.
- [8] Schellekens, P, Bos, E (in press) Aspects of Tactile Micro and Nano Probing, CIRP Internal Documents and Reports vol. 3.
- [9] Liebrich T, Knapp W, Wegener K (2009) Concept of a New 3D-probing System for Micro Components. *Proceedings of the 9th Lamdamap Conference*, 285–294.
- [10] Robinson D, Reid G (1993) *Interferogram Analysis*. Institute of Physics Publishing 0-7503-0197-X.
- [11] Gonzalez R, Woods R, Eddins S (2009) *Digital Image Processing Using Matlab*. Gatesmark Publishing 9780982085400.